Construction and Building Materials 82 (2015) 9–19

Contents lists available at ScienceDirect

Construction and Building Materials

journal homepage: www.elsevier.com/locate/conbuildmat

In-plane seismic response of rubble stone masonry specimens by means of static cyclic tests

Jelena Milosevic *, Mário Lopes, António Sousa Gago, Rita Bento

ICIST, DECivil, Instituto Superior Técnico, Universidade de Lisboa, Portugal

HIGHLIGHTS

- Characterization of mechanical behavior of the traditional rubble stone masonry.
- Experimental evaluation of displacement and strength capacity via static cyclic test.
- Analysis of the cyclic stiffness degradation, energy dissipation and viscous damping.

ARTICLE INFO

Article history:
Received 3 August 2014
Received in revised form 16 February 2015
Accepted 18 February 2015
Available online 2 March 2015

Keywords:
Rubble stone masonry
In-plane static cyclic test
Ductility
Stiffness degradation
Energy dissipation
Viscous damping

ABSTRACT

In several seismic countries, unreinforced masonry buildings are still used as residential buildings. Despite their popularity, there is a general lack of knowledge concerning the seismic behavior of such buildings. For this reason, a research programme was initiated in the framework of the SEVERES project to contribute to the understanding of the seismic behavior of such structures. In this campaign, four rubble stone masonry specimens typical of Lisbon old buildings were tested. This was done by applying static cyclic horizontal loads on top, combined with a pre-compression level, to obtain information about the failure mode, maximum displacement capacity and strength capacity. Furthermore, other features of cyclic behavior of the specimens relevant for their seismic performance, i.e., cyclic stiffness degradation, energy dissipation and viscous damping, were also analyzed and discussed.

© 2015 Elsevier Ltd. All rights reserved.

1. Introduction

Rigorous vulnerability assessment of existing buildings and implementation of appropriate retrofitting solutions are indispensable steps for preventing effects of future seismic events, as it allows minimizing the levels of physical damage, as well as reducing the loss of life and the economic impacts. Interventions must be based on surveys, diagnostic studies and on a reliable seismic assessment. In particular, appropriate mechanical characteristic, obtained experimentally, are important when deciding on the most adequate intervention strategy. Unfortunately, there is a general lack of knowledge concerning the mechanical characteristics of old masonry buildings.

While a significant amount of experimental research on rubble stone masonry specimens has been conducted applying diagonal compression tests [1–5], published literature reporting in-plane static cyclic tests on such specimens (lime stone and air lime mortar) is limited. However, some tests on specimens with similar materials have been performed. Costa et al. [6] performed *in situ* cyclic shear test of stone masonry walls from two different buildings previously damaged by seismic activity. Nevertheless, this study is focused on structures typical from Azores islands, which differ from buildings in Lisbon. Cyclic shear tests on stone masonry walls were also done by Chiostrini and Vignoli [7], Beolchini and Grillo [8], Vasconcelos [9], Silva et al. [10], Manoledaki et al. [11] Tomazevic [12] and Meta [13]. Pinho [14] carried out the compression–shear test on rubble stone masonry specimens. Corradi et al. [1] carried out an experimental study on the strength properties of double-leaf roughly cut stone walls by means of *in situ* diagonal compression and shear–compression tests.

However, Lisbon buildings have specific characteristic, which differ from buildings from other countries [15,1] and thus further tests are needed to obtain data for safety assessment studies and strengthening design. Thus, the main aim of this work is to contribute to the state of the art and attain a better insight on the

* Corresponding author at: IST DECivil, Av. Rovisco Pais, 1049-001 Lisboa, Portugal. Tel.: +351 927195525; fax: +351 218418200.
E-mail address: jelena.milosevic@ist.utl.pt (J. Milosevic).

http://dx.doi.org/10.1016/j.conbuildmat.2015.02.018
0950-0618/© 2015 Elsevier Ltd. All rights reserved.

mechanical behavior of the structural elements under horizontal loads.

For this purpose, and in the scope of a Portuguese research project (SEVERES project, http://www.severes.org), four rubble stone masonry specimens were tested by applying static cyclic horizontal loads on top combined with a pre-compression level, following the major concepts of ASTM Standard E2126-02a [16] and the work of Vasconcelos [9]. The tests provided important information about failure mode, maximum displacement capacity and strength capacity. Furthermore, other analyses that mainly characterize the behavior of the specimens under seismic loads, i.e., cyclic stiffness degradation, energy dissipation and viscous damping, were also performed and the results discussed.

Due to the fact that is really difficult to perform all tests *in situ* or to remove samples from old buildings, masonry specimens were built in the laboratory using traditional techniques and materials. Namely, four $120 \times 120 \times 40\ cm^3$ specimens were built to assess their behavior under static cyclic shear tests. Specimens were constructed with two types of mortar: hydraulic lime mortar (specimens S1 and S2, to simulate walls in less older buildings) and air lime mortar (specimens S3 and S4, to simulate traditional walls in old buildings). The specimens were tested twelve months after their construction to ensure the mortar's hardness.

2. Characterization of masonry materials

All specimens were made with roughly cut stones (Fig. 1), namely limestone, which was the most common type of stone used in Lisbon old buildings. The specimens were built with stones with variable shape and dimensions. During the construction special attention was paid on choosing the larger stones as the basic buildings units. In order to secure their best application, the stones were carefully chosen, to maximize the fitting and minimize the oscillations between them, but also to leave as few voids as possible. The remaining voids were filled with mortar and small stones. The transversal masonry texture consists of two layers of stones along the thickness of the specimens, as can be observed in Fig. 1.

It is important to mention that all panels were built according to the traditional rules by an experienced mason.

In a previous experimental campaign [17], compression tests on this type of stone were performed and the average value obtained for the compressive strength of cubic samples (10 cm edge length) was 48 MPa.

Mortar used in old masonry buildings was mostly based on air lime, since that hydraulic lime was not used often before the first decades of XX century. This experimental programme includes masonry specimens based on hydraulic lime in order to represent building which were built in an after period ("Placa" buildings) and to compare results with specimens where air lime was used.

Both types of mortar, hydraulic and air lime, were produced by Secil Martingança Company. Mix proportions for both types of mortar were made with a sand/binder ratio of 3/1. This composition was defined according to previous research works about the composition of mortars used in Lisbon Pombaline Old Town [18] and the analysis of several mortars [14]. The mechanical properties of the mortars, such as flexural and compressive strength, were obtained by experimental tests performed simultaneously with the cyclic tests.

According to the EN 1015-11 standard [19], nine prismatic specimens ($160 \times 40 \times 40$ mm) were tested for hydraulic mortar and three prismatic specimens were tested for air lime mortar; the obtained values of the flexural strength (mortar flexural strength is the mortar tensile strength obtained by bending tests), are presented in Table 1. Compression tests were also performed (on the half-prisms resulting from flexural strength test) and the obtained compressive strength for the hydraulic mortar and the air lime mortar can be seen in Table 1.

3. Cyclic shear tests

Two groups of specimens were considered, depending of the type of mortar used for their construction. Namely, the two specimens built using hydraulic mortar (S1 and S2) correspond to group 1, whereas the two other specimens built using air lime mortar (S3 and S4) were listed in group 2.

The tests were carried out with a vertical stress of 0.3 MPa (144 kN), where the value of the vertical stress was defined based on the actual state of stresses of load bearing walls in old Lisbon masonry buildings, representing an average vertical stress due to the structure self-weight at middle height of a building. Thus, the specimens were first subjected to a vertical pre-compression load, which was kept constant, as much as possible, during each test (Fig. 2). In order to keep the vertical load constant, the machine which controlled the vertical actuators was blocked in the beginning of the test when the vertical load was applied and reached the defined value. The vertically pre-stressed compressive load was applied through four steel bars (cables) (36 kN per bar), where each bar was equipped with a load cell with capacity of 100 kN, which allowed measuring the vertical load redistribution during the test. These cables, connected to the actuators, were anchored below the strong floor of the laboratory. A stiff beam on the top of the specimen was used for the uniform distribution of the vertical load. A set of steel rollers on the top of the specimen (Fig. 2)

Fig. 1. Specimens for cyclic test.

Table 1
Results for hydraulic and air lime mortar prismatic specimens.

	Number of prism	Flexural strength (MPa)	Half prism	Compressive strength (MPa)
Hydraulic mortar	Prism 1	0.38	1A	1.4
			1B	1.3
	Prism 2	0.34	2A	1.39
			2B	1.51
	Prism 3	0.33	3A	1.46
			3B	1.40
	Prism 4	0.37	4A	1.54
			4B	1.54
	Prism 5	0.32	5A	1.48
			5B	1.56
	Prism 6	0.39	6A	1.72
			6B	1.83
	Prism 7	0.36	7A	1.44
			7B	1.46
	Prism 8	0.41	8A	1.28
			8B	1.30
	Prism 9	0.31	9A	1.34
			9B	1.51
	Average	0.35		1.47
Air lime mortar	Prism 1	0.13	1A	0.81
			1B	0.85
	Prism 2	0.19	2A	0.77
			2B	0.93
	Prism 3	0.26	3A	0.82
			3B	0.71
	Average	0.20		0.82

allowed horizontal displacements of the top of the specimen with regard to the vertical actuators.

After the vertical load was applied, the horizontal load was transmitted to the top of the wall by means of a system of steel plates that was appropriately connected with steel bars. The horizontal force was applied by a screw jack of 300 kN capacity, as shown in Fig. 2.

In order to prevent sliding at the base, the specimens were fixed to a steel profile and clamped down using steel beams, which were vertically prestressed (Fig. 2).

The cyclic tests were displacement controlled by means of the horizontal LVDT connected to the left side of the specimen, as identified in Fig. 2. Each cycle at a given amplitude was repeated three times. The maximum amplitude was monotonically increased at each new group of three cycles. The displacement history of horizontal displacement vs. time was obtained with the controlled horizontal LVDT, connected to the left side of the specimens and is presented in Fig. 3.

The displacements of the specimens under cyclic loading were measured through a set of LVDTs, located as shown in Fig. 4. The vertical displacement of the top and bottom of the specimen was measured on the left hand side by transducers TSV1 and TSV7, respectively, whereas the TSV3 and TSV5 were used to measure vertical displacement on different heights of the specimen. Transducers TSH1, TSH3, TSH5 and TSH7 were instrumented on the specimen to measure horizontal displacement on different heights. The same arrangement of the LVDTs was made on the other side

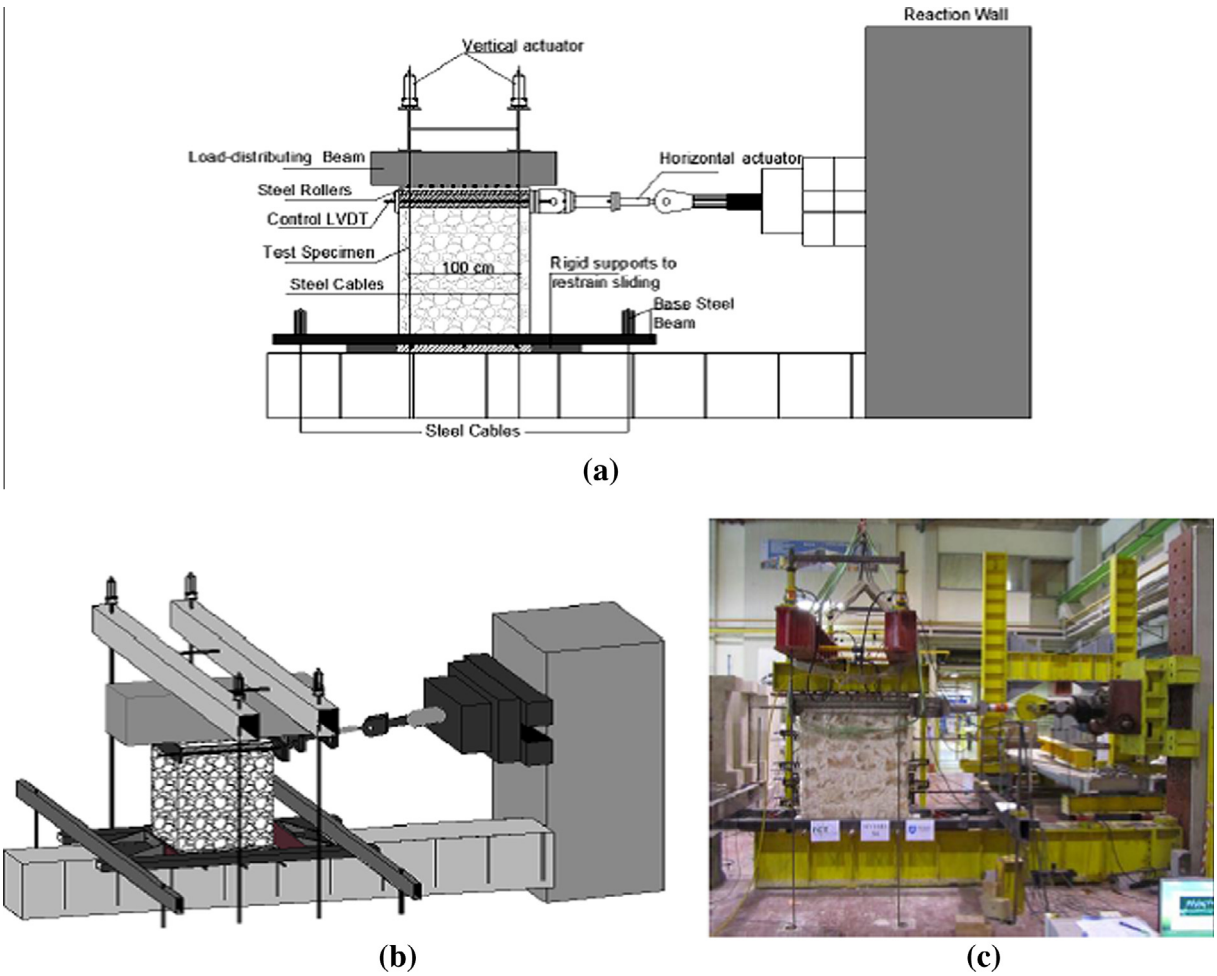

Fig. 2. Setup for cyclic shear test: (a) 2D view; (b) 3D view; (c) final setup.

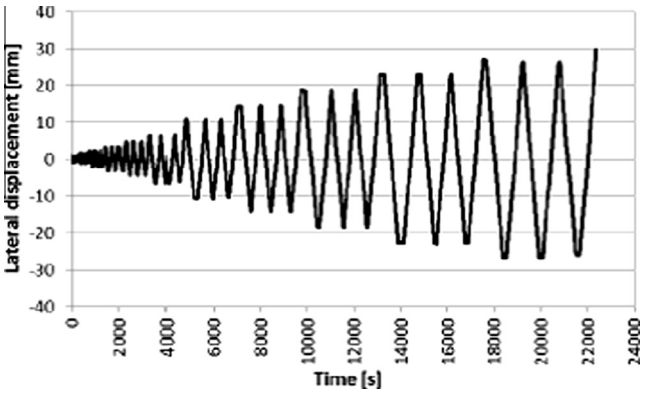

Fig. 3. Displacement history.

of the wall. It is worth to emphasize that, in order to avoid any damage of the instrumentation, all transducers (except the control one) were removed when the behavior of the specimens started to indicate that it could be close to failure. The transducers were placed on the sides in order to leave the front and back surfaces free to better observe and register the cracking process during the tests.

4. Experimental results

Cyclic test results performed on both hydraulic (group 1: S1 and S2) and air lime mortar specimens (group 2: S3 and S4) are presented and a discussion of their general behavior is reported. The presentation and discussion of the results are divided into three parts, namely: (1) discussion of the behavior and typical failure modes; (2) discussion of the typical force–displacements hysteresis diagrams and (3) evaluation of cyclic performance.

4.1. Typical behavior and failure modes

Taking account the observed seismic damage to complex masonry walls, as well as the damage obtained from laboratory experimental tests, it can be concluded that masonry specimens subjected to in-plane loading may show two typical types of behavior:

- Flexural behavior, that can be associated to the failure modes of rocking (specimens start to behave as a rigid body rotating about the edge) and crushing (characterized by a progressive and widespread damage pattern, with sub-vertical cracks oriented towards the compressed corners).
- Shear behavior, which can be related with the failure modes of diagonal cracking (where specimens usually develop cracks at the center that after propagate towards the corners) and shear sliding (failure due to sliding on a horizontal bed joint plane).

Despite this classification, combined modes are also possible. The predominance of one mode over another depends on several parameters: the panel geometry (texture, cross-section and height/width ratio), the boundary conditions, the vertical load and the mechanical characteristics of their constituents (mortar, blocks and joints) [20].

4.1.1. Masonry specimens with hydraulic mortar – Group 1

The first damage of specimen S1 takes place at small lateral displacements and is characterized by flexural cracking with the appearance of horizontal cracks on the first mortar bed joint between the specimen and the lower concrete beam (Fig. 5a). As the lateral force increased, the opening of these cracks reached larger values. After this stage, the first diagonal cracks due to the shear mechanism appeared. This first diagonal crack was developed along the stone–mortar interface in the middle of the specimen's back side (Fig. 5b), for a lateral displacement of approximately −12 mm during the load cycle of maximum displacement of −22 mm. Furthermore, a diagonal shear crack also developed in the specimens' front side and propagated towards the upper left and the bottom right corners when the imposed displacement was −26 mm (Fig. 5c). Crack damage in the stones near the shear crack was not observed. It should be mentioned that damage of specimen S1 was also characterized by a crack pattern that induced crushing on the bottom corners. As can be noticed that the final stage of failure is different for back (Fig. 5d) and front sides (Fig. 5e) of the specimen. That can be explained by different orientation of main mortar joints and by different degrees of interlocking between the stones on both faces.

In specimen S2, as in the case of specimen S1, horizontal cracks developed since early stages of displacement at the base of the specimen and progressively spread along its length (Fig. 6a). As the horizontal displacement increases, progressive damage was detected by spreading and increasing number of cracks and respective openings. The first diagonal crack was observed on the back side on the center of the specimen (Fig. 6b) and then diffused towards the top and bottom corners (only through stone–mortar interfaces) at lateral displacement around 20 mm during the load cycle after a displacement of 30 mm was reached. Additionally, the first diagonal crack on the specimen's front side appeared later (Fig. 6c), at lateral displacement approximately 10 mm during the load cycle corresponding to a peak displacement of 36 mm. Stones' sliding, clearly seen after collapse as shown in Fig. 6e), was present even before the collapse of the specimen. However, during the experimental testing, this stone sliding did not significantly affect the final collapse of the whole specimen. As can be observed in the Fig. 6 the cyclic response of the specimen S2 is predominantly influenced by flexure.

4.1.2. Masonry specimens with air lime mortar – Group 2

In case of specimen S3, the first diagonal shear crack appeared on both sides of the specimen (Fig. 7a and b) at very small horizontal displacements (roughly about 2 mm), followed by the occurrence of a large number of small cracks distributed throughout of the specimens. During the test, crack damage in the stones was not

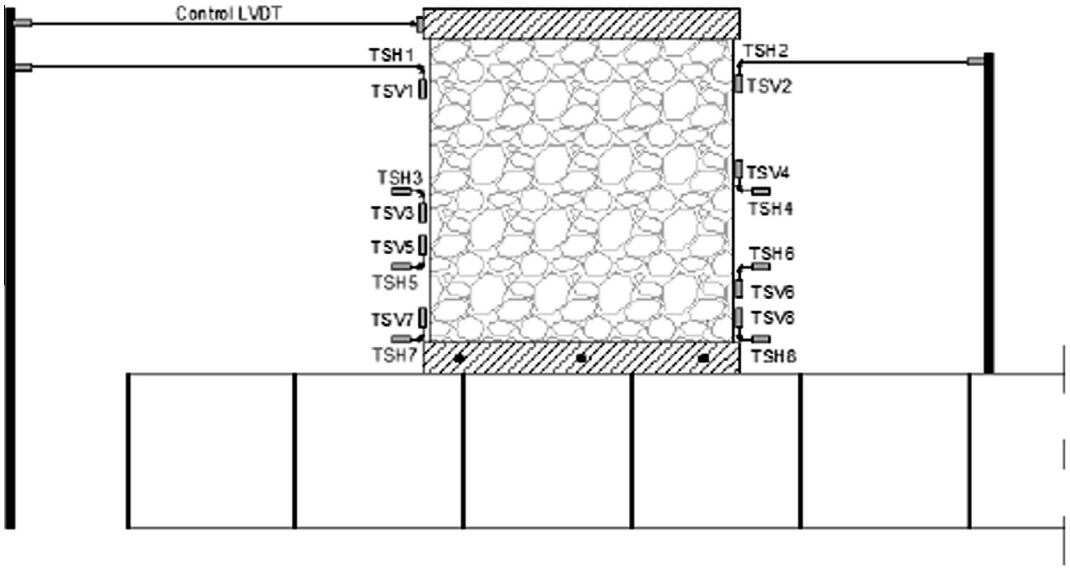

Fig. 4. Position of transducers.

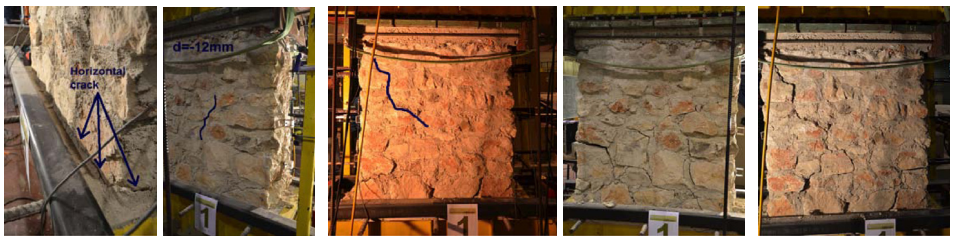

Fig. 5. Specimen S1. First visible crack (a–c). Collapse mechanism (d and e).

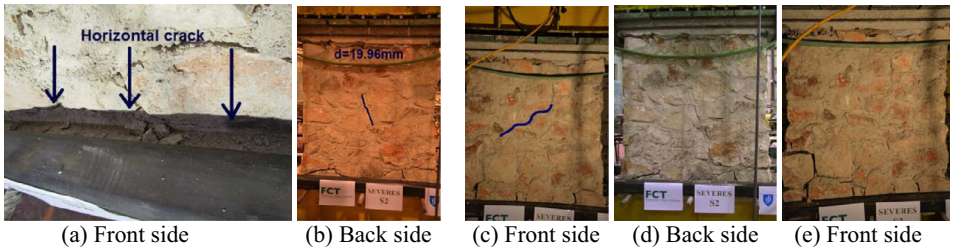

Fig. 6. Specimen S2. First visible crack (a–c). Collapse mechanism (d and e).

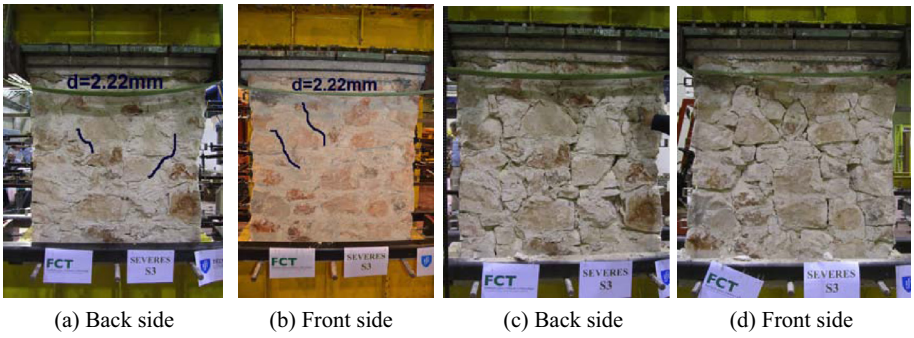

Fig. 7. Specimen S3. First visible crack (a and b). Collapse mechanism (c and d).

found and crushing of the bottom corners did not occurred, as in the specimens with hydraulic mortar. With increasing imposed displacements, the process of forming new cracks and extending the existing ones continued. At the final stage, as can be seen in Fig. 7c and d, the specimen was split in several parts.

Similarly to specimen S3, in specimen S4 at very small horizontal displacement (around 2 mm), diagonal shear cracks appeared on both sides of the specimen. The first diagonal shear crack developed close to left side of the back side of the specimen (Fig. 8a) and close to the right edge on the front side of the specimen (Fig. 8b). As the imposed displacement increases, more cracks started to appear on the both specimens' sides. At displacements of around 6 mm, clear diagonal shear cracks, which propagated towards the upper and bottom corners on both side of the specimen (Fig. 8c and d), were noticed. Subsequently, increasing the displacement gradually, the opening of these cracks reached larger values. The failure of the specimen was attributed to the crushing of the left bottom corner on the specimen's back side, as can be seen in Fig. 8c.

It is worth mention, that for specimens with air lime mortar (S3 and S4) cracks in the stone–mortar interface were visible before testing, highlighting the weaknesses of the air lime mortar (the most used in Lisbon's old buildings). Some of the cracks appeared during the mortar hardening but others may have occurred during the prototype placement in the setup. These type of damages cannot be seen in real structures due to the plaster finishing, but is to believe that real masonry walls present cracks in the mortar–stone interfaces (that occurred by mortar hardening or structural movements). Thus, the performed tests on specimens with air lime mortar are representative of existent Lisbon masonry structures.

In the walls built with hydraulic lime mortar, at the same stage of maturity, cracks were not noticed.

After the tests, for specimens from group 2 (S3 and S4) some stone units, which seemed to be still part of the specimens, were in fact detached from it and could be removed by hand.

As can be noticed in Figs. 5–8 there are differences between failure modes for specimens with hydraulic and air lime mortar. In specimens with hydraulic lime mortar, cracks are clearly defined at the final stage (before failure), whereas specimens based on air lime were completely "opened". Furthermore, in case of the specimens with air lime mortar, on one side there was an almost vertical crack "dividing" the specimen practically on two halfs (Fig. 9). In specimens with hydraulic mortar, this situation did not occur. One more difference that can be noticed is that the bottom left corner on the specimen's back side completely disintegrated for specimen with air lime mortar, whereas specimen with hydraulic mortar remained in one piece. Additionally, comparing the front and back sides of the specimens with hydraulic mortar, and taking into account the value of ultimate forces (Table 2), it can be noticed that the front side of the specimens show larger strength, comparing to the back side. This can be attributed to variability in construction.

A summary of the type of response and the failure modes observed in rubble stone masonry walls with both types of mortar (hydraulic and air lime) is given in Table 2. The type of behavior observed is also confirmed by the shape of the hysteresis diagrams presented in the following section.

4.2. Typical hysteresis diagrams

In addition to the crack patterns and failure modes, the horizontal force–horizontal displacement diagrams provide valuable information on the lateral in-plane behavior, needed to evaluate the seismic performance. In this section, a general discussion on particular features of typical diagrams is undertaken. Relevant values of the force–displacement diagrams, associated to ultimate load or damage levels are defined. The state corresponding to the maximum lateral resistance is identified with the set of values (F_{max}, d_{max}), the first shear crack is associated to the set (F_{crack}, d_{crack}) and the force and displacement at failure by $F_{failure}$ and $d_{failure}$. The results are summarized in Table 3 and the horizontal force–horizontal displace-

Fig. 8. Specimen S4. First visible crack (a and b). Collapse mechanism (c and d).

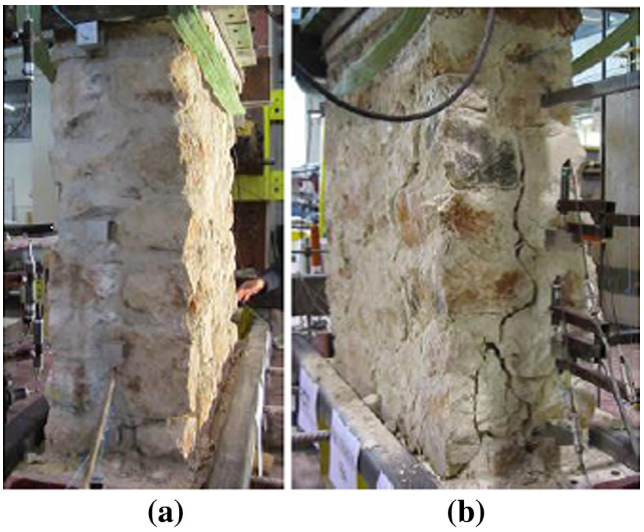

Fig. 9. Vertical crack on the specimen's side: (a) specimen with hydraulic mortar, (b) specimen with air lime mortar.

Table 2
Summary of the response/failure mode for tested specimens.

Specimen	S1	S2	S3	S4
Failure mode	Flexural/shear	Flexural	Shear	Shear

ment diagrams (where the horizontal displacement is the one recorded using the control LVDT), for hydraulic lime and air lime mortar specimens, are presented in Figs. 10 and 11, respectively.

For specimen S1, on the positive side of the curve the maximum applied load was 53.86 kN at a horizontal displacement of 6 mm. For the negative side of the curve, the maximum applied load was −82.69 kN, at a horizontal displacement of −14 mm. The force when the first shear crack was noticed was −70.24 kN (after reaching the maximum load) at a horizontal displacement of −12 mm, at a cycle of displacement amplitude −22 mm. In the case of specimen S2, the maximum load on the negative side of the curve was −92.44 kN at a horizontal displacement of −10.13 mm. The first shear crack appeared at a load of 52.38 kN (after reaching the maximum load, as in the case of specimen S1) and horizontal displacement of 19.98 mm (in a cycle of displacement amplitude 30 mm). The positive side of the curve was not considered in the analyses, due to the some irregularities which appeared: during the test, due to the movement and deformation of the specimen, one vertical actuator reached his maximum stroke. This led to the increase of the axial force on that jack which in turn created a bending moment, applied on top of the wall. Therefore the horizontal force increased to counteract this effect, as can be seen in Fig. 10b. If it was not for this, the behavior would be expected to be similar to the one registered in the opposite direction and in test for specimen S1.

In case of specimens with hydraulic mortar, (S1 and S2), the tests were stopped at a stage in which it seems the wall was about to fail, with some large stones completely separated from the rest of the wall. At this stage the load was around 95% of max horizontal load (Fig. 10a and b). Results can be seen in Table 3.

It is important to say that at the moment of application of vertical load, before any horizontal displacement was applied, in the case of specimens with hydraulic mortar (S1 and S2), an horizontal force of around 20 kN was registered, which is one of the reason of the asymmetric in the respective graphics (Fig. 10). This initial horizontal force was due to an asymmetry in the test setup, which was solved in the following tests of air lime specimens.

Concerning specimen S1, the hysteresis diagram is associated with the mixed deformation composed of flexural and shears cracking, which is in agreement with the failure pattern. A similar behavior of masonry specimens was observed by Silva et al. [10]. The higher asymmetry in the cyclic response, namely at the level of the maximum lateral strength observed in this specimen (S1), besides the above mentioned asymmetry in the test set-up, can be attributed to the different damage patterns of the specimen's sides (flexural and shear).

The lateral response of the specimen S2 is governed more by a flexural crack pattern and large displacements can be attained without significant loss of strength. In the case of this specimen, there is an obvious asymmetry of the force–displacement diagram. This can be explained with the fact that cracking initiated earlier in the direction of positive displacement and therefore, as a result of the higher damage accumulation, the respective specimen side was weakened more rapidly.

Furthermore, as can be noticed, for the two specimens (S1 and S2), the differences in the maximum lateral strength are minimal. Additionally, in larger amplitude cycles after the maximum load, there is a little strength degradation for both specimens.

The maximum load for specimen S3 was 43.79 kN, registered at an horizontal displacement of 10.84 mm and −42.84 kN, registered at an horizontal displacement of −4.75 mm for positive and negative sides of the curve, respectively, as can be seen in Fig. 11a. First shear crack appeared at a load of 30.72 kN and horizontal displacement of 2.90 mm (cycle of displacement amplitude 2 mm). Maximum load for specimen S4 for the positive side of the curve was 42.68 kN registered at an horizontal displacement of 6.52 mm and −38.94 kN at a horizontal displacement of −3.74 mm for the negative side of the curve. The first shear crack appeared at a load of −33.82 kN at a horizontal displacement of −2.21 mm (cycle with displacement amplitude 2 mm), this is, before the maximum load was attained. In the case of specimens with air lime mortar (S3 and S4) failure load was considered as 80% of the maximum previous horizontal load, and results are presented in Table 3. As expected, specimens built with air lime mortar showed much lower strength than the specimens based on hydraulic lime mortar. They also showed much less deformation capacity.

Comparing the specimens' behavior, the specimens with air lime mortar (S3 and S4, displayed in Fig. 11a and b), show less deformation capacity and lateral resistance than what was presented by the hydraulic lime mortar specimens. Moreover, for the specimens with hydraulic mortar degradation of strength is almost negligible, while in case of specimens with air lime mortar, the strength at the end of the tests is almost half the values of maximum lateral strength, and differences in the maximum lateral strength between specimen S3 and S4 are insignificant.

Furthermore, the specimen's collapse from group 2 was achieved without damage in the stones, i.e., the cracks propagated only through the mortar joints, which also shows that mortar type has major influence in the specimen behavior.

Regarding the energy dissipation it can be noticed that specimens with hydraulic lime mortar dissipate much more energy than specimens built with air lime mortar.

4.3. Evaluation of the cyclic performance

Due to the complexity of the seismic response of old structures, in order to perform adequate seismic assessment and to propose safe and economical design of retrofitting measures, a better understanding of the factors that affect the hysteretic behavior is really important. The bilinear idealization curve representing the nonlinear monotonic behavior and parameters such as ductility, energy dissipation, cyclic stiffness, equivalent viscous damping ratio and lateral drifts characterize the behavior of shear walls and are helpful in evaluating the performance of a structure under seismic loading. These will be presented in the following section for the specimens previously analyzed.

Table 3
Cyclic shear tests.

Specimen	Left						Right					
	F_{crack} (kN)	d_{crack} (mm)	F_{max} (kN)	d_{max} (mm)	$F_{failure}$ (kN)	$d_{failure}$ (mm)	F_{crack} (kN)	d_{crack} (mm)	F_{max} (kN)	d_{max} (mm)	$F_{failure}$ (kN)	$d_{failure}$ (mm)
S1	70.24	12.0	82.69	14.0	80.32	26.84	–	–	53.86	6.0	47.57	30.0
S2	–	–	92.44	10.13	89.24	36.59	52.38	19.98	Not relevant			
S3	–	–	42.84	4.75	34.27	10.72	30.72	2.90	43.79	10.84	35.04	14.82
S4	33.82	2.21	38.94	3.74	31.15	6.45	–	–	42.68	6.52	34.14	10.72

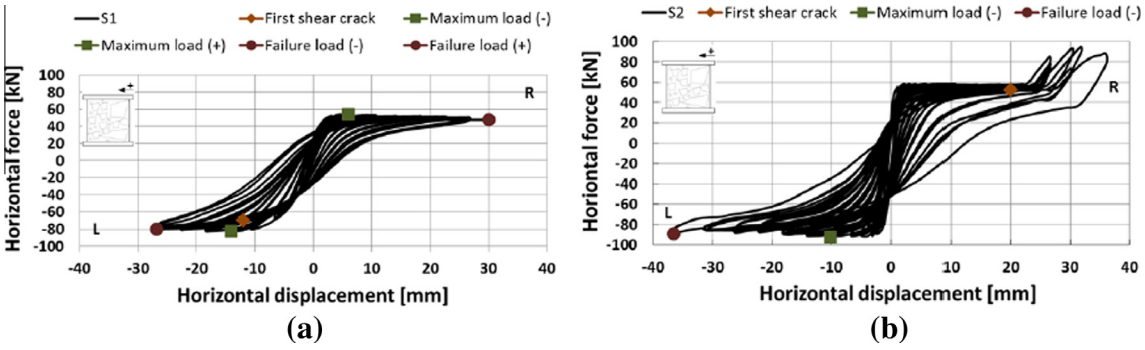

Fig. 10. Group 1 – walls with hydraulic lime mortar: horizontal force vs. horizontal displacement: (a) S1; (b) S2.

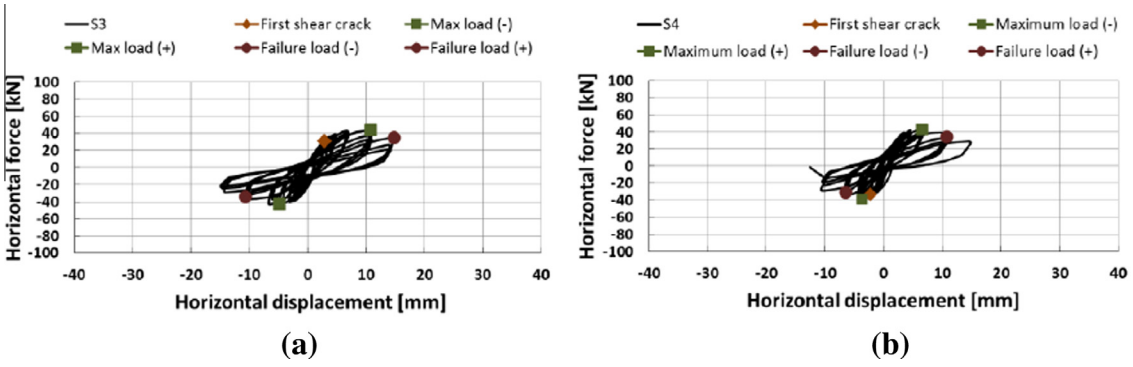

Fig. 11. Group 2 – walls with air lime mortar: horizontal force vs. horizontal displacement: (a) S3; (b) S4.

4.3.1. Bilinear idealization

The force–displacement relationship registered in shear cyclic tests is usually presented in the shape of hysteresis loops. In order to quantify the overall behavior of specimens the evaluation of the envelopes of the hysteresis loops and its bilinear idealization is firstly performed. The bilinear idealization procedure has been widely reported in the literature as a simplified method of evaluating the seismic parameters of masonry specimens under cyclic loading (Magenes and Calvi [21]; Bosiljkov et al. [22]; Eurocode 8 [23]).

According to Tomazevic [20] three limit states need to be defined in order to idealize the experimental envelope (Fig. 12a): the crack limit corresponding to the stage where the first significant cracks appears (H_{cr}, d_{cr}), the maximum resistance identified by the couple (H_{max}, $d_{H\ max}$) and the ultimate state, related to the maximum displacement attained during the cyclic test d_u. In this study H_{cr} was considered as 70% of H_{max}, according to the Italian standard [24].

The initial stiffness is calculated as the ratio between the lateral force, H_{cr} and lateral deformation, d_{cr} by the following expression:

$$K_e = \frac{H_{cr}^{+} - H_{cr}^{-}}{d_{cr}^{+} - d_{cr}^{-}} \tag{1}$$

The ultimate resistance H_u of the idealized bi-linear response was calculated, taking into account the requirement that the energy dissipation capacity of the experimentally obtained and idealized response be equal (Fig. 12a). After calculating the stiffness and area under the experimental envelope A_{env}, the ultimate resistance can be calculated from [20] as:

$$H_u = K_e\left(d_{max} - \sqrt{d_{max}^2 - \frac{2A_{env}}{K_e}}\right) \tag{2}$$

The corresponding yield displacement is:

$$d_y = \frac{H_u}{K_e} \tag{3}$$

The ultimate idealized displacement (d_u) corresponds to the point where strength reaches 80% of H_{max}, as proposed in both Italian standard [24] and EC8 [23]. In case of specimens with hydraulic mortar, (S1 and S2), the maximum displacement d_{max} is used instead of d_u, since that there is no significant load degradation of the masonry.

Ductility is an important factor for the evaluation of the seismic behavior of structures in seismic regions, as it is directly related to the ability of the structure to deform nonlinearly without significant loss of strength. Ductility is defined here as the ratio between the ultimate displacement (d_u) and the yield displacement (d_y) defined in the equivalent bilinear diagram:

$$\mu = \frac{d_u}{d_y} \tag{4}$$

In the following work, the monotonic envelope curves are defined as the curve connecting the points of maximum load in the hysteresis plot at each displacement level. Due to the low variations obtained during the tests among the three repetitions of cycles, the envelope curves were plotted only for the first cycles at each displacement amplitude. Due to the differences in the behavior between two specimen's sides, envelopes in both directions were selected for the calculation of seismic parameters. It should be noted that in case of specimen S2, only the negative side envelope was considered, due to the fact that some irregularities appeared on the positive side of the curve (see explanation in Section 4.2). The obtained bilinear idealized curves are shown in Fig. 12b.

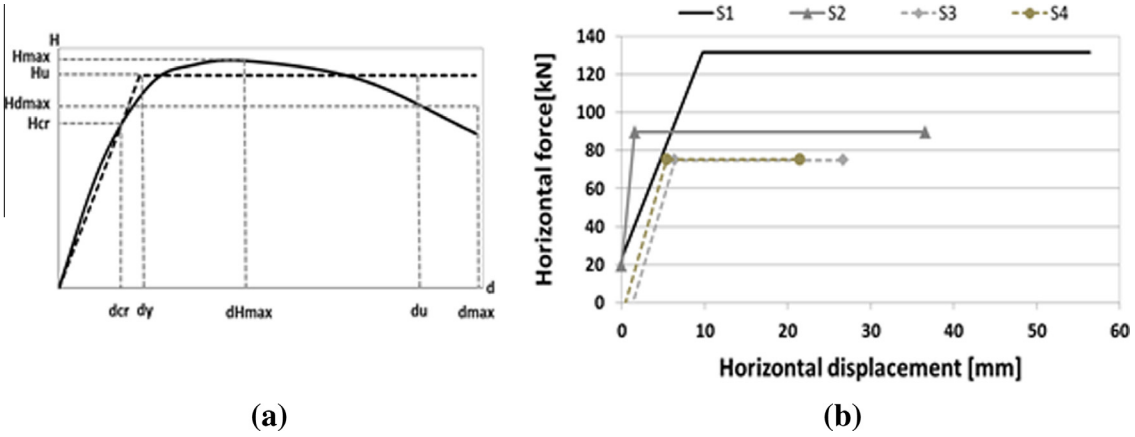

Fig. 12. Bilinear curves of tested specimens: (a) method used to obtain the bilinear curves; (b) bilinear idealizations for all specimens.

The values that define the envelopes and of the corresponding bilinear idealization defining each limit state of the specimens S1, S2, S3 and S4 are summarized in Table 4.

It is important to mention that for both specimens with air lime mortar (S3 and S4), ultimate load H_u is around 90% of H_{max}. This finding is in agreement with the value reported by Tomaževic [20] as the average value of the idealized ultimate resistance obtained from more than 60 tests on walls failing in shear. For specimens with hydraulic mortar (S1 and S2) the relation between ultimate H_u and maximum load H_{max} is $H_u \approx 0.96H_{max}$ what can be explained by the fact that specimen S1 has flexural/shear failure mode and specimen S2 failed in flexural mode where the, strength degradation of the envelope is minimal.

In all specimens the stiffness and ductility clearly depends of failure mode. In case of specimens with hydraulic mortar (S1 and S2) high differences of stiffness and ductility can be found. This can be explained by the fact, that in case of specimen S1, the two specimen's sides were governed with different failure modes, namely one side failed in shear, whereas in the other one flexural mode was prevailed. In case of specimen S2, the relatively high values of the stiffness and ductility factor are the result of the cyclic response being governed only by flexural patterns. Moreover, orientation of the mortar joints and interlocking between stones can also be the reason of these high values obtained. Furthermore, in case of specimen S2, only the negative side was taken into account during the evaluation of parameters due to the irregularities, which appeared during the test, what can also explain the differences in results with specimen S1. On the other hand, the values for stiffness and ductility for specimens failed in shear (S3 and S4), are similar.

Anyway, note should be made concerning the scattering on the results: it was only possible to build and test a reduced number of specimens and the scatter is influenced by the dispersion of the failure mode and textural variability.

4.3.2. Energy dissipation and stiffness degradation

Besides the ductility, one important parameters used for the assessment of the seismic performance of the seismic behavior is the ability of a structural element to dissipate energy during cyclic nonlinear deformations. A dissipative structure can mean the reduction of the seismic response and, consequently, the reduction of the ductility demand [25].

The energy that is dissipated at each loading cycle, E_{diss}, is obtained by calculating the area enclosed by the loop in the load–displacement diagram (Fig. 13a). The energy needed to deform the wall up to an imposed lateral displacement is called input energy, E_{input}, and is calculated as the sum of areas under the positive and negative branches of the hysteresis loop, see Fig. 13b).

Figs. 14 and 15 show the variation of the dissipated energy per each cycle for all specimens and the evolution of dissipated energy with the increasing lateral drift.

As can be noticed, the increase on the dissipated energy per cycle is related to the increase of damage as the lateral drift increases. This is naturally associated to the propagation of damage in a structure and with the increase of the displacement. In fact, by its definition, large dissipation of energy is equivalent to high energy inside the hysteresis loop, which is associated with the maximum displacement amplitude and the shape of the loops. However, it is noticed that the evolution of dissipated energy is not directly proportional to the lateral displacements. The sudden increase of the dissipated energy is almost always associated to the full opening of diagonal cracks, such as in specimen S3 for lateral drift (which was calculated as the ratio between the lateral top displacement and the height at which the lateral load is applied) of 0.57% and 0.91% (load cycle n° 15 to n° 17 – marked with circles) or in specimen S4 for a lateral drift of 0.55% and 0.89% (load cycle n° 16 to n° 17 – marked with squares). Similar observations were also found by Vasconcelos [9]. Comparing the two specimens of hydraulic mortar (S1 and S2) it can be noticed that specimen S2 has slightly higher amounts of dissipated energy than S1, due to its higher load capacity. Moreover, as can be seen in Fig. 14, for specimens S1 and S2, a much more regular (linear) increase rate of dissipated energy was found when compared with the specimens S3 and S4. This feature is in agreement with the flexural and mixed flexural/shear failure mechanism that governs the cyclic in-plane lateral response of these specimens. Moreover, in case of specimen S1 and S2, there is no sudden increase of the dissipated energy as in specimens S3 and S4 that failed in shear. Furthermore, from the two groups of tested specimens (group 1 with hydraulic and group 2 with air lime mortar), it is clear that specimens based on hydraulic mortar (group 1: S1 and S2) have significant bigger amount of dissipate energy due to the higher load bearing capacity.

The equivalent viscous damping ratio is correlated to energy dissipation. Damping is the process by which the amplitude of free vibrations steadily diminishes [26]. Equivalent viscous damping is calculated according to Eq. (5) [21]:

$$\xi_{eq} = \frac{E_{diss}}{2\pi(E^{+}_{input} + E^{-}_{input})} \quad (5)$$

where E_{diss} is the dissipated hysteretic energy, E^{+}_{e} and E^{-}_{e} are the energies needed to deform the specimen up to the imposed lateral displacement (input energies) and they are calculated as the sum of areas under positive and negative branches of the hysteresis loop (Fig. 13). As shown in Fig. 16a for specimens with hydraulic mortar, there is a great variation of damping for low values of lateral drift, whereas for larger values of lateral drift (approximately between 0.5% and 2%), damping becomes almost constant. On the other side, for specimens with air lime mortar (Fig. 16b), increasing of damping can be noticed. This different behavior is related to the different global behavior of the specimens. Magenes and Calvi [21] concluded that for specimens with a flexural behavior (in this case S1 and S2) the values of damping are almost constant, while for a diagonal shear cracking response (S3 and S4) the values are usually increasing with an increase of drift and accumulated damage. Nevertheless same average values of equivalent viscous damping could be suggested for specimens with hydraulic lime mortar, 4–5%, and 10% for walls with air lime mortar. The low values of ξ_{eq} obtained for S1 and S2 were expected, mainly due to the narrow shape of the hysteretic curves, related to their flexural or flexural–shear behavior, associated to the fact that the flexural mechanism of resistance degrades much less due to the cyclic nature of the load history than the shear type of mechanism.

Table 4
Characteristic values of the hysteretic envelopes.

Specimen	H_{cr} (kN)	d_{cr} (mm)	K_e (kN/mm)	d_e (mm)	H_u (kN)	d_u (mm)	H_{max} (kN)	$d_{H\ max}$ (mm)	μ
S1	95.58	7.0	13.5	9.75	131.59	56.39	136.54	20.48	5.78
S2	64.71	1.15	50	1.59	89.63	36.59	92.44	10.13	22.9
S3	60.64	5.2	11.6	6.42	75.01	26.70	86.64	15.58	4.16
S4	57.13	4.1	13.9	5.4	75.30	21.44	81.62	10.26	3.96

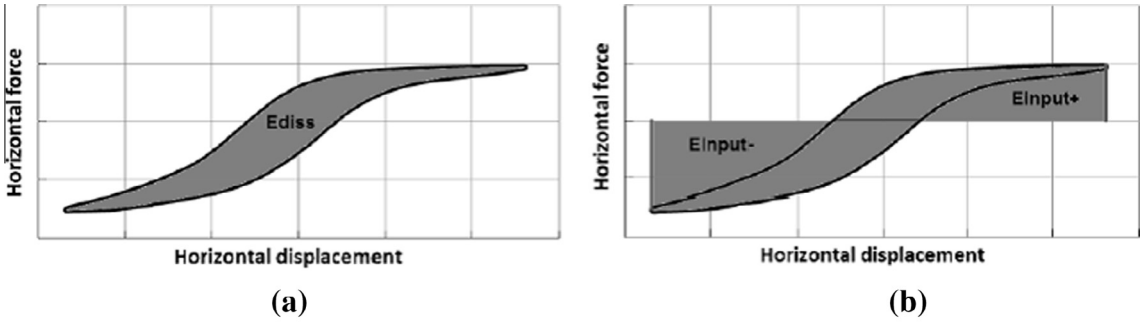

Fig. 13. Evaluation of energy in one loading cycle; (a) dissipated energy; (b) input energy.

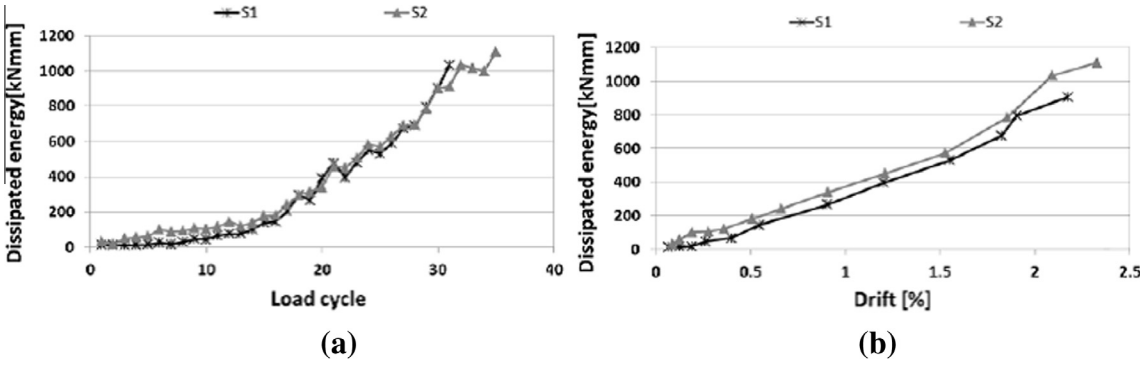

Fig. 14. Evolution of dissipated energy for specimens S1 and S2: (a) for each cyclic loop; (b) as a function of lateral drift.

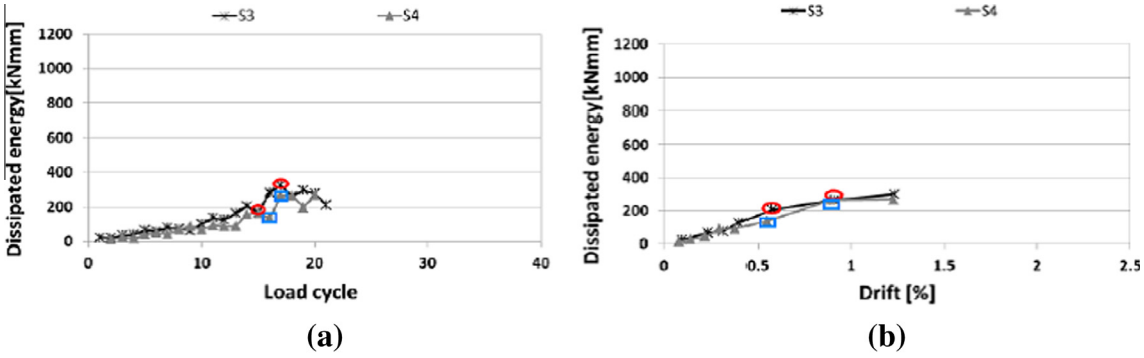

Fig. 15. Evolution of dissipated energy for specimens S3 and S4: (a) for each cyclic loop; (b) as a function of lateral drift.

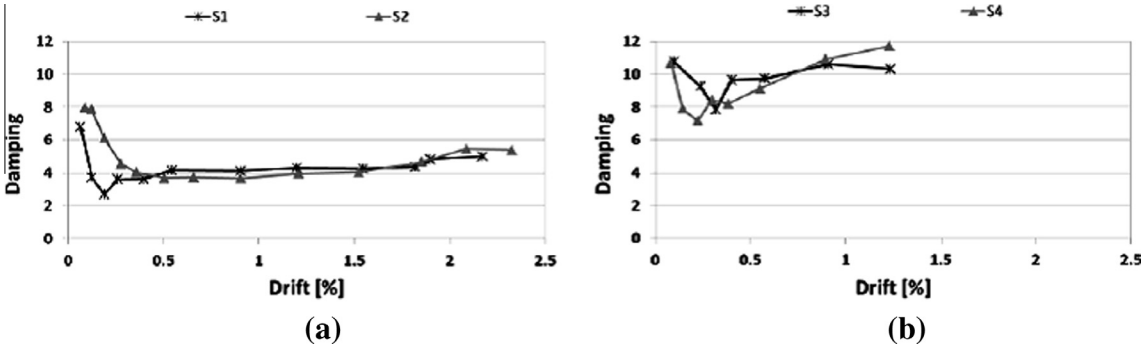

Fig. 16. Values of equivalent viscous damping as a function of the drift: (a) specimen S1 and S2; (b) specimen S3 and S4.

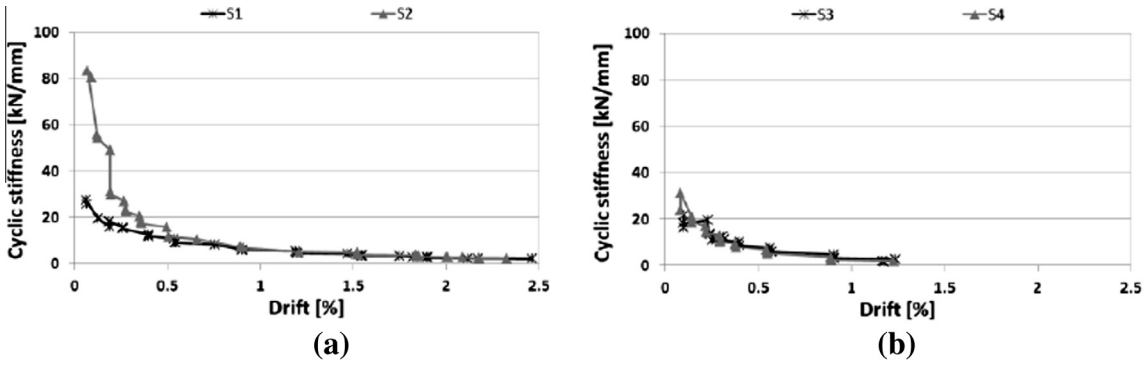

Fig. 17. Degradation of the cyclic stiffness: (a) specimen S1 and S2; (b) specimen S3 and S4.

Table 5
Cyclic test – literature review.

Masonry type	Ductility μ	Stiffness K (kN/mm)	Estimation of the stiffness	Authors
Rubble stone masonry, hydraulic lime mortar	3.37	–	–	Silva et al. [10]
Rubble granite stone masonry, lime mortar	2.60 2.08	6.53 6.92	Ratio between the estimated force on the cracking point and corresponding displacement	Arede et al. [28]
Rubble granite stone masonry, lime mortar	2.55	7.69	Ratio between average of the ultimate load (H_u) and corresponding displacement	Almeida et al. [29]
Rubble stone masonry, lime mortar	–	18.33	Ratio between the force of first significant crack and corresponding displacement	Tomazevic et al. [12]
Rubble granite stone masonry, air lime mortar	12.09	11.52	Ratio between the force of first significant crack and corresponding displacement	Vasconcelos [9]
Three-leaf stone masonry walls (lime stone, lime mortar)	4.17 3.41	–	–	Meta et al. [13]
Rubble stone masonry, hydraulic lime	5.78 22.9	13.5 50	The ratio between the lateral force, H_{cr} and lateral deformation d_{cr} (Eq. (1))	Current work (2014)
Rubble stone masonry, air lime	4.16 3.96	11.6 13.9	The ratio between the lateral force, H_{cr} and lateral deformation d_{cr} (Eq. (1))	Current work (2014)

In order to evaluate the degradation of stiffness during the cyclic tests, cyclic stiffness was assessed by calculating stiffness for each loading cycle as the slope of the straight line that connects origin and the points of maximum and minimum horizontal load obtained from the force–displacement diagrams [27]. In this case only average values between the calculated stiffness of positive and negative slope is presented for all tested specimens. Due to the stabilization of cycles in the beginning of the tests, for low values of displacement there were some uncertainties and because of that reason, values of cyclic stiffness for first two cycles should be analyzed with caution. As shown in Fig. 17 for hydraulic and air lime mortar specimens, significant decreasing on the values of lateral stiffness appears as the lateral drift increases. As already mention, the lateral drift was calculated as the ratio between the lateral top displacement and the height at which the lateral load is applied. It is worth mention that main stiffness degradation occurs for lateral drifts lower than 0.5%, as can be noticed in Fig. 17. It can also be noted that in the case of specimens of hydraulic mortar (S1 and S2), cyclic stiffness has an almost constant value after value of drift 1.5%, while the specimens with air lime mortar did not reach these deformation levels. These results show, once again, the importance of the mortar in the cyclic behavior of the walls.

For the purpose of comparison Table 5 summarizes some published results obtained by cyclic tests on masonry built with materials similar to the materials used in the specimens S1, S2, S3 and S4. For the current work (whose values are in the last two rows) two values of ductility and stiffness are depicted in each cell, corresponding to the values obtained for each of the two specimens of hydraulic and air lime mortar tested. The scatter between presented results can be explained by different ways of building the specimens and theirs textural variability. Furthermore, different way of calculation of the stiffness is also the reason for the differences in results.

5. Conclusions

The study of existing masonry structures and their seismic vulnerability represents the key point in the structural rehabilitation process of old buildings. In spite of some recent studies, the characterization of the structural behavior of stone masonry walls subjected to seismic actions is not completed, in fact we are far from that.

This is one of the first works that thoroughly analyzes rubble stone masonry specimens, similar to the old buildings from Lisbon, namely with lime stone and air lime and hydraulic lime mortar. Several conclusions can be drawn from these tests:

- The stones' layout has great influence on the overall behavior of the specimens, as two specimens based on hydraulic mortar presented different behavior. Specimen S1 is characterized by mixed shear/flexural failure mode, whereas other specimen had a flexural behavior.
- The mortar type has a huge influence of the results: specimens built with air lime mortar showed much lower strength than the specimens built with hydraulic lime mortar.
- Regarding the energy dissipation it can be noticed that specimens with hydraulic lime mortar dissipate much more energy than specimens built with air lime mortar.
- In all specimens the stiffness and ductility clearly depends of failure mode, the specimen S2, showed relatively high values of the stiffness and ductility which resulted from the fact that the cyclic response was governed by flexural patterns, whereas, in the specimen S1, where mixed failure mode were reached lower values were obtained. The specimens made with air lime mortar, S3 and S4, both failed in shear, presenting similar values for stiffness and ductility.

- For specimens with hydraulic mortar, there was a great variation of damping for low values of lateral drift, whereas for larger values of lateral drift damping becomes almost constant. However, for specimens with air lime mortar, continuous increasing of damping was noticed. The difference in the global behavior of the specimens is related to the fact that, in air lime mortar specimens the internal degradation continues more extensively at higher deformations. Furthermore, different values were obtained: small for specimens S1 and S2 and higher for specimens S3 and S4, are also related with the behavior and failure mode of the specimens, namely pure shear in the specimens based on air lime mortar and mixed shear–flexural in case of specimens with hydraulic mortar.

Acknowledgments

The authors acknowledge the financial contribution of FCT (*Fundação para a Ciência e a Tecnologia*) to the project SEVERES: "Seismic Vulnerability of Old Masonry Buildings" (www.severes.org).

References

[1] Corradi M, Borri A, Vignoli A. Experimental study on the determination of strength of masonry walls. Constr Build Mater 2003;17:325–37. http://dx.doi.org/10.1016/S0950-0618(03)00007-2.
[2] Corradi M, Tedeschi C, Binda L, Borri A. Experimental evaluation of shear and compression strength of masonry wall before and after reinforcement: deep repointing. Constr Build Mater 2008;22:463–72. http://dx.doi.org/10.1016/j.conbuildmat.2006.11.021.
[3] Brignola A, Frumento S, Lagomarsino S, Podestà S. Identification of shear parameters of masonry panels through the in-situ diagonal compression test. J Archit Herit 2008;3:52–73. http://dx.doi.org/10.1080/15583050802138634.
[4] Borri A, Castori G, Corradi M, Speranzini E. Shear behaviour of unreinforced and reinforced masonry panels subjected to in situ diagonal compression tests. Constr Build Mater 2011;25:4403–14. http://dx.doi.org/10.1016/j.conbuildmat.2011.01.009.
[5] Milosevic J, Gago AS, Lopes M, Bento R. Experimental assessment of shear strength parameters on rubble stone masonry specimens. Constr Build Mater 2013;47:1372–80. http://dx.doi.org/10.1016/j.conbuildmat.2013.06.036.
[6] Costa AA, Arêde A, Costa A, Oliveira CS. In situ cyclic tests on existing stone masonry walls and strengthening solutions. Earthquake Eng Struct Dyn 2011;40:449–71. http://dx.doi.org/10.1002/eqe.1046.
[7] Chiostrini S, Vignoli A. In-situ determination of the strength properties of masonry walls through destructive shear and compression tests. Proceedings of International Workshop on Effectiveness of Injection Techniques for Retrofitting of Brick and Stone Masonry Walls in Seismic Areas. p. 253–82.
[8] Beolchini GC, Grillo F. In situ tests of stone masonry panels. Proceedings of International Workshop on Effectiveness of Injection Techniques for Retrofitting of Brick and Stone Masonry Walls in Seismic Areas 1992:197–205.
[9] Vasconcelos G. Experimental investigations on the mechanics of stone masonry: characterization of granites and behaviour of ancient masonry shear walls [Ph.D. thesis]. Portugal: University of Minho; 2005.
[10] Silva B, Benetta MD, Porto F, Modena C. Experimental assessment of in-plane behavior of three-leaf stone masonry walls. Constr Build Mater 2014;53:149–61.
[11] Manoledaki AA, Drosos V, Anastasopoulos I, Vintzileou E, Gazetas G. Experimental assessment of the seismic response of three-leaf stone masonry walls, with due consideration to soil–structure interaction. Proceedings of the 15th World Conference on Earthquake Engineering (15WCEE), Lisbon, Portugal.
[12] Tomazevic M, Gams M, Berset T. Seismic strengthening of stone masonry walls with polymer coating. Proceedings of the 15th World Conference on Earthquake Engineering (15WCEE), Lisbon, Portugal.
[13] Meta K, Mark M, Bokan-Bosiljkov V, Bosiljkov V. Seismic retrofitting of three-leaf stone masonry walls by means of grouting and NSM glass cords. Proceedings of the 9th International Masonry Conference (9IMC), Guimarães, Portugal.
[14] Pinho FFS, Baião MFC, Lúcio VJG, Faria P. Experimental research on rubble stone masonry walls. HMC08 Historical Mortars Conference – LNEC, Lisbon – September.
[15] Mendes N, Lourenco BP. Seismic assessment of masonry "Gaioleiro" buildings in Lisbon, Portugal. J Earthquake Eng 2009;14(1):80–101.
[16] ASTM E 2126-02a. Standard test methods for cyclic (reversed) load test for shear resistance of walls for buildings. ASTM International: West Conshohocken, PA; 2002, 19428–2959.
[17] Carvalho J. Mechanical characterization of loadbearing masonry stone through non-destructive testing (in Portuguese) [Master's thesis]. Lisbon: Instituto Superior Técnico; 2008.
[18] Nero J, Appleton J, Gomes A. As Argamassas Tradicionais no Parque Edificiado de Lisboa: Uma Colaboração para o seu Conhecimento. 2 Encontro sobre conservação e reabilitação de edifícios, LNEC, Lisboa.
[19] CEN: 1015-11: 1999. Methods of test for mortar for masonry-Part 11: determination of flexural and compressive strength of hardened mortar; 1999.
[20] Tomazevic M. Earthquake-resistant design of masonry buildings. London: Imperial College Press; 1999, ISBN 1-86094-066-8.
[21] Magenes G, Calvi GM. In-plane seismic response of brick masonry walls. J Earthquake Eng Struct Dyn 1997;26:1091–112.
[22] Bosiljkov V, Page A, Bokan-Bosiljkov V, Žarnic R. Performance based studies of in-plane loaded unreinforced masonry walls. Masonry Int 2003;16:39–50.
[23] European Committee for Standardization (CEN). Eurocode 8: design of structures for earthquake resistance – Part 3: assessment and retrofitting of buildings (EC8-3); 2005.
[24] Italian Code for Structural Design, D.M. 14.01.08, Official Bullettin no. 29 of [04.02.08 in Italian].
[25] Shing PB, Noland JL, Klamerus E, Spaeh H. Inelastic behavior of concrete masonry shear walls. J Struct Eng 1989;115:2204–25.
[26] Chopra AK. Dynamics of structures Chopra A. Englewood Cliffs, New Jersey: Prentice Hall; 1995.
[27] Zepeda JA, Alcocer SM, Flores LE. Earthquake-resistant construction with multiperforated clay brick walls. Proceedings of the 12th World Conference on Earthquake Engineering. p. 1541–8.
[28] Arede A, Mendes P, Silva B, Guedes J, Faria J, Costa A. Experimental assessment of a seismic strengthening solution for stone masonry walls using a wooden structure. Proceedings of the 14th World Conference on Earthquake Engineering (14WCEE).
[29] Almeida C, Guedes JP, Arede A, Costa A. Shear and compression experimental behavior of one leaf stone masonry walls. Proceedings of the 15th World Conference on Earthquake Engineering (15WCEE), Lisbon, Portugal.